

Numerical Modelling of the Hydrodynamic Performance of Sinusoidally Pitching Hydrofoils

A. Dubois, Z. Q. Leong, H. D. Nguyen and J. R. Binns

Australian Maritime College
 University of Tasmania, Tasmania 7248, Australia

Abstract

The collective and cyclic pitch propeller (CCPP) is a novel efficient and effective propulsion and manoeuvring alternative for Autonomous Underwater Vehicles (AUVs). A two-dimensional numerical model was developed to investigate the hydrodynamic performance of the CCPP, simplifying the three-dimensional CCPP's blade operation to that of two-dimensional pitching hydrofoils. The hydrodynamic performance of the hydrofoils was defined by the degree of asymmetry and unsteady evolution of the generated forces over the azimuthal cycle, identified in earlier CCPP research as key in the control of the resulting manoeuvring forces and AUV motion. The model development established a numerically efficient and space-time independent solution procedure and validated the model's ability to predict the effects of parametric pitch variations on the azimuthal asymmetry of the generated forces.

Introduction

In recent years the use of Autonomous Underwater Vehicles (AUVs) has become an important part of underwater exploration and reconnaissance. The diversity in deployment purposes and mission profiles of AUVs requires a combination of efficient, long-range travelling capabilities with effective operation at low speeds [1]. Considering traditional control surfaces lose their efficiency at low speeds and low speed manoeuvring aids such as side- or podded-thrusters reduce the long-range travelling efficiency, a design issue arises. A possible propulsion and manoeuvring alternative, addressing both issues, is the implementation of a propeller capable of collective and cyclic pitch control.

Helicopter flight control inspired the implementation of collective and cyclic blade pitch control to be used for the propulsion and manoeuvring of marine vehicles. By changing the propeller blade's pitch angle simultaneously (collective) and periodically over the azimuthal cycle (cyclic), a single propeller becomes capable of generating omni-directional forces, and consequently AUV motion, in three degrees of freedom: surge, pitch and yaw. Through collective and cyclic pitch control, the propeller concept is able to adjust for unsteady blade loads [4] and, more importantly, provide efficient propulsion and effective manoeuvring forces at both zero and non-zero forward speeds [2, 7] for a wide range of marine vehicles.

Recent experimental research on a collective and cyclic pitch propeller (CCPP) for a torpedo-shaped AUV (see figure 1), demonstrated the concept's capability of generating usable manoeuvring forces [3, 9]. However, results of the experimental work revealed a phase shift between the orientation of the intended side-force and the effective, generated side-force, identified as well in earlier research [2, 7]. Additional CCPP research [8] further stressed the need for increased understanding of the origins, evolution and unsteady character of the side-force phase shift in order to ensure effective and accurate force vectoring and consequently AUV manoeuvring.

The current study aims to investigate the unsteady flow behaviour involved in CCPP operation and understand the ef-

fects of collective and cyclic pitch variations on the resulting side-force magnitude and orientation. By using Computational Fluid Dynamics (CFD) and simplifying the CCPP's three-dimensional blade motion to two-dimensional pitching hydrofoils, a numerical model was developed. The numerical model, aimed at investigation and quantification of the side-force phase shift, was verified and validated for future use as two-dimensional analysis tool of the CCPP's hydrodynamic performance.

Methodology

CCPP Working Principle

The working principle of the CCPP is fairly simple. Through cyclic, sinusoidal variation of the propeller blades' pitch the generated forces change over the azimuthal cycle ϕ_{azi} (see figure 2). The cyclic variation results in a force imbalance over the cycle, effectively generating a pitching / yawing moment turning the AUV. Essential in the effective manoeuvring of the AUV is the propeller rake β (see figure 3). Implementation of a blade rake angle allows for the generation of an actual side-force besides the turning moment inherently caused by the imbalance at zero rake.

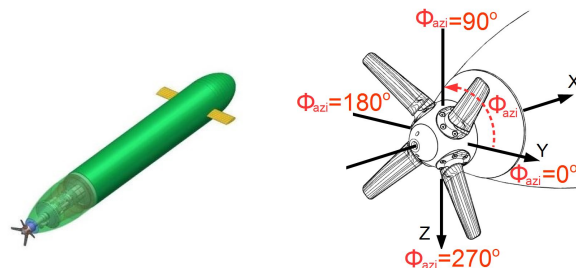


Figure 1: Torpedo-shaped AUV with CCPP [3].

Figure 2: Definition of azimuthal blade cycle.

Control of the size and orientation of the force imbalance is key in effectively manoeuvring an AUV using the CCPP. Current CCPP control assumes a one-to-one linear relation between the sinusoidally varying azimuthal blade pitch and the generated forces, without taking into account unsteady flow effects. Additional asymmetry of the force distribution, i.e. the lift and drag distribution $L(\phi_{azi})/D(\phi_{azi})$, over the azimuthal cycle as a result of the dynamic flow will also influence the force imbalance. Unsteady flow effects thereby directly pose an issue for the side-force orientation and consequently for the resulting AUV motion.

Force Break-Down

The CCPP undergoes a constant rotation around the x-axis and has multiple blades, four in this case. One can thus assume that the lift and drag generated by one blade over the azimuthal cycle represents the overall net lift and drag distribution generated by all blades together over the cycle (assuming negligible blade-to-blade interaction). In order to assess the resulting forces $F_{x,y,z}$

the lift and drag are decomposed based on azimuthal blade position and the blade rake angle, as seen in equations (1), (2) and (3) and defined in figure 3.

$$F_x(\phi_{azi}) = L(\phi_{azi}) \cdot \cos(\beta) \quad (1)$$

$$F_y(\phi_{azi}) = L(\phi_{azi}) \cdot \sin(\beta) \cdot \cos(\phi_{azi}) - D(\phi_{azi}) \cdot \sin(\phi_{azi}) \quad (2)$$

$$F_z(\phi_{azi}) = L(\phi_{azi}) \cdot \sin(\beta) \cdot (-\sin(\phi_{azi})) - D(\phi_{azi}) \cdot \cos(\phi_{azi}) \quad (3)$$

The net forces are defined as the averaged forces over the azimuthal cycle, with the side-forces orientated in y - and z -direction. The vector sum of the side-forces results in the effective side-force, quantified by the side-force magnitude F_s and angle $\phi_s = \angle(F_y, F_z)$.

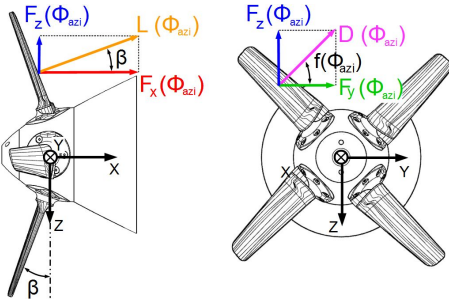


Figure 3: CCPP force break-down.

Two-Dimensional Simplification

The performance of the three-dimensional pitching CCPP blades was simplified to that of a two-dimensional, sinusoidally pitching hydrofoil. By using a two-dimensional prediction of the generated lift and drag, the three-dimensional performance can be analysed with considerable simplification. The three-dimensional collective and cyclic pitch is related to the two-dimensional mean pitch ψ_0 and pitch amplitude $\Delta\psi$, respectively. Further matching is done based on the Reynolds number $Re = \frac{\rho U c}{\mu}$ (defined by the apparent flow speed U over the CCPP blades and the hydrofoil's chord length c) and the reduced pitch frequency $k = \frac{2\pi f_p \cdot \frac{c}{U}}{2}$ (based on the pitch frequency f_p). Evaluation of the hydrodynamic performance was based on the resulting side-force phase shift $\gamma_s = \angle(\phi_{int}, \phi_s)$ (with the intended side-force angle ϕ_{int}) and the asymmetry of the azimuthal lift and drag distribution responsible for the side-force orientation.

Numerical Model

Model Outline and Solver Settings

The flow over the two-dimensional pitching hydrofoil is simulated using the flow solver FLUENT16.0, by solving the Unsteady Reynolds-averaged Navier–Stokes equations (URANS). Based on the flow characteristics and recommendations found in literature [6, 10], the $k-\omega$ SST transition model, with a curvature correction, was used to model the flow turbulence.

Time discretisation was done using a second-order bounded, implicit dual-time stepping method. The pressure-based solver used a least-square cell based PISO-algorithm for the pressure-velocity coupling and second order (upwind) discretisation was applied for the pressure, momentum and turbulence modelling parameters. Finally, flow initialisation was done based on the flow velocity over the foil and to ensure the solution's independence of start-up effects three pitch oscillations are performed before evaluation of the actual performance.

Flow Domain and Boundary Conditions

The computational domain was split up into two parts (see figure 4), which allowed for the inner domain to rotate, simulating the hydrofoil's pitching motion and the outer domain remaining stationary. Both domains were linked through a sliding mesh interface. A c-routine was used to specify the sinusoidal pitching motion of the hydrofoil. The domain dimensions were set at 6 chord lengths in front, above and below the hydrofoil and 12 chord lengths behind it.

The following boundary conditions were applied: inlet as a uniform velocity inlet (perpendicular to boundary), outflow condition for the outlet, symmetry conditions for the sides, no-slip condition on the hydrofoil, and a matching boundary condition at the sliding interface. The fluid density ρ was specified as 998.2 kg/m^3 and the dynamic viscosity μ as $1.003 \times 10^{-3} \text{ kg/(m}\cdot\text{s)}$.

Spatial and Time Discretisation

A structured grid, consisting of quadrilateral elements, was created using Pointwise and dimensioned based on the number of cells over the hydrofoil's chord. The mesh strategy in the inner domain is shown in figure 5. Other mesh specifications include a first layer $y+$ of 1, inflation layers with a maximum growth rate of 1.2 around the hydrofoil to capture the boundary layer, and cell size transition over the interface and different domain parts did not exceed an area ratio of five. The time discretisation parameters were established during the convergence study.

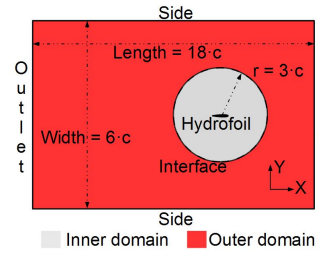


Figure 4: Fluid domain set-up and

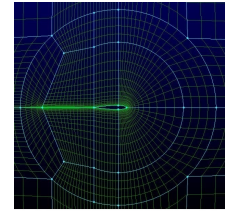


Figure 5: Spatial discretised grid.

Case Selection

For the verification and validation of the numerical model experimental work by Lee and Gerontakos was used [5]. The experimental work investigated the characteristics of the unsteady boundary layer and stall events occurring on foil oscillating under different pitch conditions. Table 1 gives an overview of the flow and pitch conditions of the experimental work, which were chosen based on matching of the three-dimensional to two-dimensional conditions.

Parameter	Value	Parameter	Value
Foil type	NACA0012	k	0.025–0.2
Pitch-point	1/4-chord	ψ_0	0° – 15°
Re	1.35×10^5	$\Delta\psi$	0° – 15°

Table 1: Foil, flow and pitch parameters as used in the experimental work by Lee and Gerontakos [5].

Convergence Study

By evaluating the influence of the numerical spatial and time discretisation parameters, the convergence study established the dependency of the solution (and model) of the applied discretisation. The solution convergence was evaluated based on the

calculated side-force phase shift defined as the angle between the effective side-force and the intended orientation of the side-force, as determined by the intended direction of AUV motion.

Based on recommendations found in literature [10] and trial runs, the initial physical time-step Δt was set at based on a number of steps N per pitch period T_p (equivalent to a percentage n of the characteristic flow time $T_c = \frac{c}{U}$), established to be $N = 800$ and $n = 0.04$, respectively. The initial grid resolution was verified based on simulations of a static foil under an angle of attack and was determined to require 122 cells over the hydrofoil's chord (160k cells over the entire domain).

Time Convergence

Evaluation of the convergence of the dual-time stepping included analysis of both the inner numerical steps and the outer physical time-step. The sensitivity of the solution to the number of inner time-steps was evaluated based on the convergence of the continuity equation. Figure 6a shows that a convergence tolerance of 10^{-4} was sufficient with the side-force phase shift changing less than 1% with finer convergence tolerance levels.

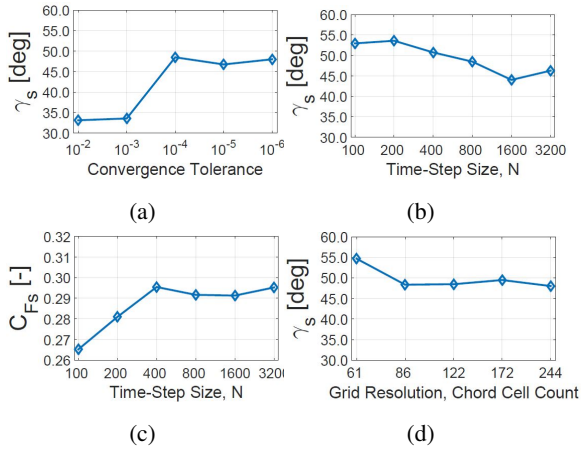


Figure 6: Convergence study – side-force phase shift / magnitude as a function of (a) the convergence tolerance, (b) / (c) the time-step size and (d) the grid resolution.

Analysis of the physical time-step was done over seven time-step levels, based on the pitch period and / or the characteristic flow time. In figure 6b the side-force phase shift is plotted against the number of time-steps per pitch period (equivalent to characteristic flow time levels of $n = 0.32; 0.16; 0.08; 0.04; 0.02; 0.01$, respectively). Time convergence of the side-force phase shift appeared less clear, with the solution varying around 10% around the mean value over the time-steps, most likely due to the massive unsteadiness present in the flow. Inspection of the convergence of the side-force magnitude, added in figure 6c and other evaluation parameters, such as the impulse over the different azimuthal quadrants, did more clearly show convergence over the time-step levels. Based on the closer investigation the initial time-step ($N = 800; n = 0.04$) showed to be sufficiently refined for the current purposes.

Spatial Convergence

Five grid resolutions were tested at the determined convergence tolerance and physical time-step (10^{-4} and $N = 800 / n = 0.04$, respectively), comparing the initial grid resolution to two coarser and two finer grids. The number of cells over the hydrofoil chord were 61, 86, 122, 172 and 244 with a total cell count of 40k, 80k, 160k, 320k and 640k, respectively. The calculated side-force phase shifts showed to converge within 1%

on the coarse grid (86 cells over chord length), shown in figure 6d, which was therefore selected as appropriate for future calculations.

Spatial-Time Convergence

Finally, the initial time-step and grid resolution was varied simultaneously to investigate the space-time convergence of the model. Results of the calculated side-force phase shift showed to be varying less than 5%. Considering the complex and unsteady character of the flow, the found error can be considered a reasonable engineering tolerance and the solution method was established as space-time independent.

Validation Study

The numerical modelling approach was then applied to a number of additional cases to investigate its capabilities in simulating the hydrodynamic performance of pitching hydrofoils. Besides analysis of the verification case, referred to as the benchmark case, three more cases were simulated. The different cases tested the model's ability to capture changes in the hydrodynamic performance when operating under different conditions. Both changes of the reduced frequency and pitch parameters were tested, as seen in table 2.

Case name	Re	k	ψ_0	$\Delta\psi$
Benchmark	1.35×10^5	0.1	10°	15°
Validation 1	1.35×10^5	0.05	10°	15°
Validation 2	1.35×10^5	0.05	0°	7.5°
Validation 3	1.35×10^5	0.05	0°	15°

Table 2: Overview of verification and validation cases.

Benchmark Case

Analysis of lift and drag coefficient profile $C_{L/D} = \frac{L/D}{\frac{1}{2}\rho U^2 c}$ of the benchmark case, presented in figure 7, showed good overall agreement between the numerical and experimental results. Although the lift peak was not fully captured, a slight over-prediction of the lift minimum and over-prediction of the drag maximum, the model showed to be able to predict the overall force evolution.

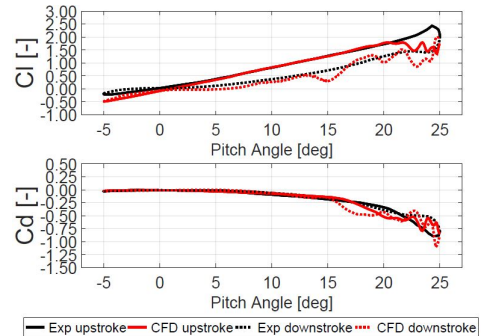


Figure 7: Benchmark case – comparison of experimental and numerical lift and drag coefficient variation over the pitch angle.

Figure 8 further shows the asymmetry of the azimuthal force distribution through comparison of the time-integral of the lift and drag coefficients over the four azimuthal quadrants J (quadrant definition: $Q_I = 0-90^\circ; Q_{II} = 90-180^\circ; Q_{III} = 180-270^\circ$ and $Q_{IV} = 270-360^\circ$). The distribution of impulse over the four quadrants provides insight in how the resulting side-forces will be orientated by visualising the force imbalance over the cycle. The results showed the ability to capture the overall

trend(s), most importantly capturing the asymmetry between Q_I and Q_{II} of the lift coefficient within 10% accuracy. Further trends, e.g. the asymmetry of lift and drag impulse of $Q_I + Q_{II}$ vs. $Q_{III} + Q_{IV}$, are generally predicted within a similar range of accuracy. Despite minor discrepancies, primarily as a result of over-prediction of the lift coefficient at negative pitch angles and inability to capture the full unsteadiness of flow occurring during the down-stroke, the model proofed its ability to predict the asymmetry of the azimuthal force distribution.

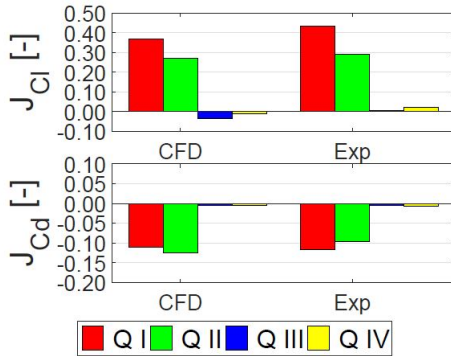


Figure 8: Benchmark case – comparison of experimental and numerical impulse distribution of the lift and drag coefficient.

Further Validation Cases

All four validation cases were evaluated based on the calculated side-force orientation and magnitude, seen in figure 9 from which the side-force phase shift can be derived by the visualisation of the intended side-force orientation. The numerical results showed that the model captured the effects of the parametric variations in side-force magnitude and deviations from the intended side-force orientation, i.e. side-force phase shift, relatively well. Remaining differences between the experimental and numerical results were attributed, after further analysis, to over-prediction of the numerical lift coefficient and inaccuracies in the conversion of the available experimental data (data digitized from plots with limited accuracy).

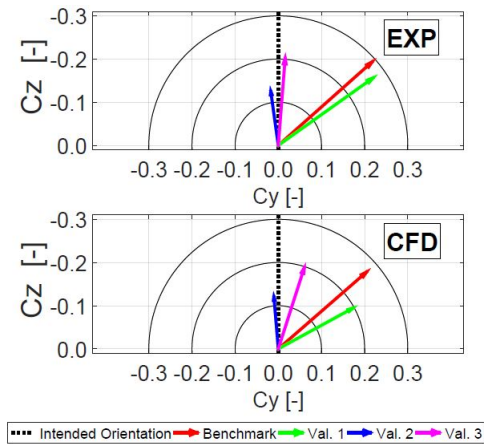


Figure 9: Validation of side-force magnitude and orientation.

Conclusions and Future Work

The current research established a numerical methodology for future investigation of the hydrodynamic performance of sinusoidally pitching hydrofoils as a tool for the analysis of the side-force phase shift occurring in CCPP operation. Through verification the numerical approach was established to reach a con-

verged, numerically independent solution with a convergence tolerance of 10^{-4} for the continuity equation, a time-step equal to 1/800 of the pitch frequency and 4% of the physical flow time, and at least 86 cells over the hydrofoil's chord length. The validation study showed the ability of the model to capture the azimuthal asymmetry of the generated forces and predict the influence of parametric pitch variations on the occurring side-force phase shift. Thereby, the model provides insight in the unsteady flow phenomena involved in the operation of pitching hydrofoils and can be used as tool for further analysis.

Future work involves the use of the numerical model to analyse the evolution of the side-force phase shift over a wide range of collective and cyclic pitch variations, including comparison with experimental CCPP results. Combined with the development of a full three-dimensional model, for which the current model will serve as basis, the research aims to further investigate, understand, explain, and address the occurring side-force phase shift and hydrodynamic CCPP performance in general.

References

- [1] Chyba, M., Autonomous underwater vehicles, *Ocean Engineering*, **36**, 2009, 1 – 1.
- [2] Haselton, F. R. and Rice, R. S., Tandem propeller concept of submarine propulsion and control, *Journal of Aircraft*, **3**, 1966, 180–184.
- [3] Humphrey, T. C., Bose, N., Williams, C. and Snow, M., Design and fabrication of a collective and cyclic pitch propeller, in *ASME 2004 23rd International Conference on Offshore Mechanics and Arctic Engineering*, American Society of Mechanical Engineers, 2004.
- [4] Jessup, S. D., *Reduction of propeller vibration and cavitation by cyclic variation of blade pitch*, Master's thesis, Massachusetts Institute of Technology, 1976.
- [5] Lee, T. and Gerontakos, P., Investigation of flow over an oscillating airfoil, *Journal of Fluid Mechanics*, **512**, 2004, 313–341.
- [6] Martinat, G., Hoarau, Y., Braza, M., Vos, J. and Harran, G., Numerical simulation of the dynamic stall of a NACA 0012 airfoil using DES and advanced OES/URANS modelling, in *Advances in Hybrid RANS-LES Modelling*, Springer, 2008, 271–278.
- [7] Murray, B., Fraser, J., Dai, C. and Maskew, B., Applications of cyclic pitch thrusters, in *Propellers/Shafting '94 Symposium*, Society of Naval Architects and Marine Engineers, Virginia Beach, Virginia, 1994.
- [8] Nguyen, H. D., Niyomka, P., Binns, J., Bose, N. and Le, K. D., Omnidirectional control of an underwater vehicle equipped with a collective and cyclic pitch propeller, in *The Second Vietnam Conference on Control and Automation*, 2013.
- [9] Niyomka, P., Bose, N., Binns, J. and Nguyen, H., Experimental characterization of collective and cyclic pitch propulsion for underwater vehicle, in *The 3rd International Symposium on Marine Propulsors, Launceston, Tasmania*, 2013.
- [10] Wang, S., Ingham, D. B., Ma, L., Pourkashanian, M. and Tao, Z., Numerical investigations on dynamic stall of low reynolds number flow around oscillating airfoils, *Computers & Fluids*, **39**, 2010, 1529–1541.